Calculated Optoelectronic Properties of Ruthenium Tris-bipyridine Dyes Containing Oligophenyleneethynylene Rigid Rod Linkers in Different Chemical Environments

M. J. Lundqvist,[†] E. Galoppini,[‡] G. J. Meyer,[§] and P. Persson*[,†,||]

Department of Quantum Chemistry, Uppsala University, Box 518, SE-75120 Uppsala, Sweden, Department of Chemistry, Rutgers University, 73 Warren Street, Newark, New Jersey 07102, Department of Chemistry, Johns Hopkins University, Baltimore, Maryland 21218, and Department of Chemical Physics, Lund University, Box 124, SE-22100 Lund, Sweden

Received: July 5, 2006; In Final Form: October 31, 2006

Ruthenium tris-bipyridine dyes containing oligophenyleneethynylene (OPE) rigid rod linker groups ($[Ru(bpy)_3]^{2+}$, $[Ru(bpy)_2bpy\text{-}E\text{-}Ipa]^{2+}$, $[Ru(bpy)_2bpy\text{-}E\text{-}Ph\text{-}E\text{-}Ipa]^{2+}$, and $[Ru(bpy)_2bpy\text{-}E\text{-}Bco\text{-}E\text{-}Ipa]^{2+}$, where bpy = 2,2′-bipyridine, E = ethynylene, Ph = *p*-phenylene, Bco = bicyclo[2.2.2]octylene, and Ipa = isophthalic acid) have been investigated using DFT and TD-DFT calculations to elucidate the influence of the rigid rod on their optoelectronic properties. Experimentally observed differences in the optical absorption for the different complexes are discussed on the basis of TD-DFT simulated absorption spectra. A comparison of the calculated optoelectronic properties of $[Ru(bpy)_2bpy\text{-}E\text{-}Ph\text{-}E\text{-}Ipa]^{2+}$ in different chemical environments, that is, in different solvents and with or without counter ions, suggests that both the absorption spectra and the redox properties of the dyes with OPE rods are sensitive to the environment. The calculations show that spurious low-energy charge-transfer excitations present in the TD-DFT calculations of the extended systems in vacuum are removed when the environment is included in the calculations.

Introduction

Many dyes based on functionalized ruthenium(II) tris-bipyridine chromophores are excellent photoactive reducing agents, characterized by a favorable combination of strong absorption of visible light, and long-lived excited states with high reducing power. These properties can initiate photocatalytic and photochemical conversion reactions in which an excited dye molecule donates an electron to an acceptor, which can be either another molecule or a solid substrate.[1−3] Such photoinduced electron-transfer processes have found widespread applications, for example, in the conversion of solar energy into electricity in dye-sensitized solar cells (DSSCs).[4−6] In most of these devices, ruthenium dyes are functionalized with designated anchor groups such as carboxylic acids, so that they can be covalently bound to a wide band gap semiconductor, such as nanostructured TiO_2, to form the working electrode.[5]

Surface electron transfer accompanying the initial light absorption and excitation of ruthenium dyes often results in efficient photoinduced charge-separation across the dye−TiO_2 interfaces.[7−17] In some of the most efficient photoinduced electron-transfer reactions reported to date, this is facilitated by the anchor group, which is able to act as a mediator of the electron transfer between the chromophore and the semiconductor substrate through delocalization of the excited state of the chromophore onto the anchor group.[13,18]

For ruthenium(II) tris-bipyridine complexes, the combination of ultrafast (∼few tenths of a femtosecond) electron injection times, long-lived (∼microsecond) excited-state lifetimes, and slow (∼millisecond) interfacial charge recombination times results in a high probability for electron injection after the initial photoexcitation of the dye to generate a long-lived charge-separated state across the molecule−metal oxide interface. Insertion of spacer groups between the chromophore and the anchor group offers an attractive way to modify the interfacial electron-transfer kinetics without seriously affecting either the favorable optical properties of the chromophore or the stable binding of the anchor groups to metal oxide substrates.[19] An important objective is to slow down detrimental charge recombination reactions, while maintaining fast forward electron injection. The effects of different spacer groups on DSSC interfacial electron-transfer rates have therefore recently been investigated both experimentally[20−22] and theoretically.[23] The dye−spacer−anchor−semiconductor arrangement can be described schematically as a heterosupramolecular donor−bridge−acceptor system, as shown in Figure 1. In terms of the interfacial electron-transfer kinetics, it is interesting to consider to what extent the spacer and anchor parts of the system together act as an electronic bridge from the donor chromophore to the semiconductor acceptor, for example, through delocalization of the chromophore frontier orbitals onto the linker.[23] For clarity, in this paper we call spacer (S) the moiety that is placed between the anchoring groups (A) and the dye, and rigid rod linker the part of the molecule that contains both the spacer and the anchoring groups, as illustrated in Figure 1.

Rigid rods have recently been introduced as spacer groups into DSSC systems, as they are expected to offer superior structural control as compared to flexible spacer groups containing, for example, saturated hydrocarbon chains.[19,24,25] This is potentially very useful both for the rational design of molecular devices[19] and for studies of the distance dependence of long-range electron-transfer kinetics. Several sensitizers containing oligophenyleneethynylene (OPE) rigid rods have been synthe-

* Corresponding author. E-mail: petter.persson@chemphys.lu.se.
[†] Uppsala University.
[‡] Rutgers University.
[§] Johns Hopkins University.
[||] Lund University.

10.1021/jp064219x CCC: $37.00
Published on Web 02/06/2007

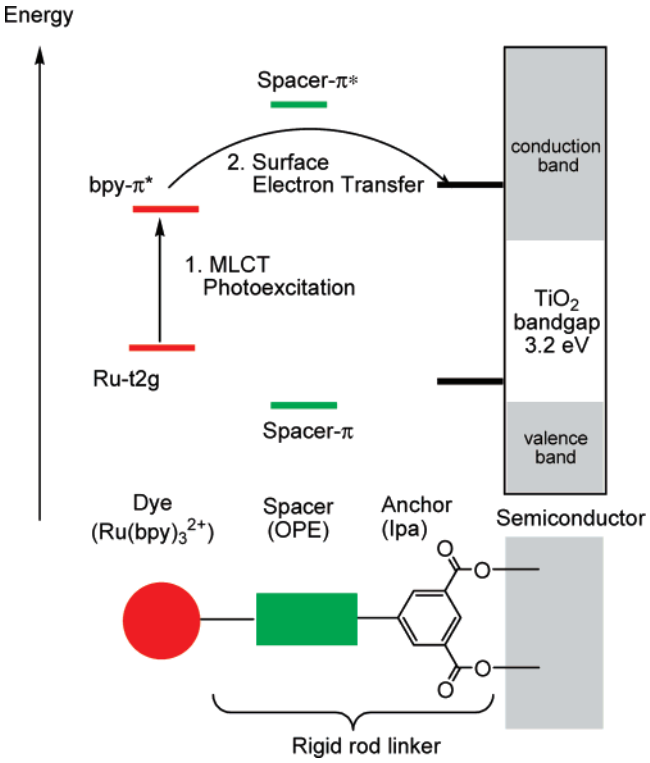

Figure 1. Schematic illustration of a dye-sensitized semiconductor interface, with the chromophore attached to the semiconductor via a rigid rod linker. The upper part of the figure shows a typical energetic alignment of the active molecular energy levels and the semiconductor band structure, and the lower part of the figure shows the corresponding structural arrangement.

sized.[21,22] Recombination has been measured for three conjugated OPE rod complexes and was found to be second-order with average rate constant, $k_{obs} \approx 10^7$ s^{-1}, and it was independent of the rigid-rod length.[22] However, the fact that it was independent could be an effect of the specific conditions studied.

An improved understanding of the dependence of electron-transfer rates on the chemical nature of the spacer is, furthermore, of significant interest to a wide range of charge-transfer processes at the molecular level in the emerging field of molecular electronics.[26] OPE spacers have in this wider context been used in several studies as a link between a variety of donor and acceptor moieties including both molecular[27] and metallic centers.[28]

In response to the significant experimental efforts to develop DSSCs and related photoelectrochemical devices, several quantum chemical investigations have been performed to provide a better theoretical understanding of the basic physical and chemical processes at dye-sensitized semiconductor interfaces.[17] This includes quantum chemical investigations of a significant number of ruthenium polypyridine dyes presented over the last several years. As a prototype complex, $[Ru(bpy)_3]^{2+}$ has been subject to several theoretical investigations.[29−33] Some calculations of ruthenium dyes have also included modeling of the solvent in the calculations, for example, to explain experimentally observed solvatochromic shifts.[34,35] It has recently also become possible to explicitly include nanocrystalline substrates such as TiO_2 in the modeling of DSSC interfaces containing ruthenium dyes.[36] It is frequently assumed that the substrate is not necessary to understand the functionality of different dyes in DSSCs, although the strong electronic interaction of sensitizers bound to TiO_2 can also give rise to direct charge-transfer excitations across the molecule−metal oxide interface,[37] as well as significant rearrangement of the electronic structure of the

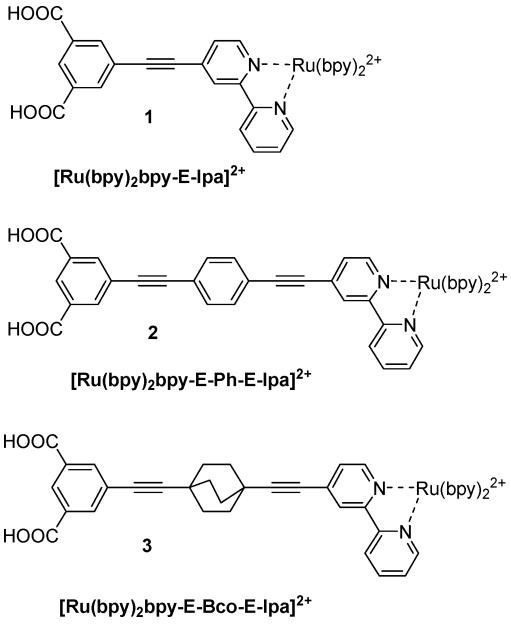

Figure 2. The chemical structures of $[Ru(bpy)_2bpy\text{-}E\text{-}Ipa]^{2+}$ (**1**), $[Ru(bpy)_2bpy\text{-}E\text{-}Ph\text{-}E\text{-}Ipa]^{2+}$ (**2**), and $[Ru(bpy)_2bpy\text{-}E\text{-}Bco\text{-}E\text{-}Ipa]^{2+}$ (**3**).

sensitizer itself.[18] In cases where such effects can be anticipated, the explicit inclusion of the substrate is likely to be essential to the modeling.[17]

Here, we discuss the role of rigid rods in dye−spacer−anchor arrays on the basis of quantum chemical calculations. A comparison of the absorption spectra of the $[Ru(bpy)_3]^{2+}$, $[Ru(bpy)_2bpy\text{-}E\text{-}Ipa]^{2+}$ (**1**), $[Ru(bpy)_2bpy\text{-}E\text{-}Ph\text{-}E\text{-}Ipa]^{2+}$ (**2**), and $[Ru(bpy)_2bpy\text{-}E\text{-}Bco\text{-}E\text{-}Ipa]^{2+}$ (**3**) series of complexes, shown in Figure 2, is first made to provide information about the development of features in the optical absorption spectra related to the size and conjugation of rigid rod linkers. This is complemented by a more extensive investigation of complex **2** using DFT and TD-DFT calculations, to provide a detailed theoretical understanding of the optoelectronic properties of a prototype dye-rigid rod system in different chemical environments.[38]

Methods

Density functional theory (DFT) and time-dependent DFT (TD-DFT) calculations have been performed using, primarily, the B3LYP hybrid functional[39] together with the LANL2DZ effective core potentials (ECP) and accompanying basis set.[40] All calculations were performed using the Gaussian 03 program[41] and, unless noted otherwise, using the B3LYP/LANL2DZ combination of DFT functional and ECP/basis set.

Initially, the ground-state geometries of all of the molecules ($[Ru(bpy)_3]^{2+}$, **1**, **2**, and **3**) were optimized assuming a low-spin electronic structure with a net positive charge (+2) due to the presence of the Ru(II) ion. Absorption spectra of the complexes in acetonitrile, including all singlet excitations with wavelengths longer than 250 nm, were subsequently simulated using the TD-DFT approach with the default polarized continuum model (PCM) for this solvent.[42] The theoretical absorption spectra were generated using an arbitrary Gaussian peak broadening of 10 nm. TD-DFT calculations of singlet excitations were also performed without solvent.

A more detailed theoretical comparison was made between complex **2** and the parent complex $[Ru(bpy)_3]^{2+}$ to investigate the influence of conjugated linkers on the optoelectronic properties of ruthenium complexes. This included optimizing the two molecules both in their respective singlet ground state

(S0), oxidized doublet state, as well as the triplet state with lowest energy (T1).

The effect of the environment was furthermore studied by calculations explicitly including two PF_6^- counter ions to obtain a formally neutral overall system in the calculations of the complexes $[Ru(bpy)_3]^{2+}$ and **2** in their respective Ru(II) states. The two counter ions were placed in grooves present between the bipyridyl ligands in the optimized dyes. The combined dye−counter ion systems were subsequently fully reoptimized in the gas phase. In particular, oxidation of a rigid rod dye was considered by explicitly optimizing $[Ru(bpy)_3]^{2+}$ and **2** as doublets.

In an attempt to investigate the properties of the lowest triplet state, and thus also some of the effects of excited-state relaxation, an estimation of the lowest triplet state of **2** was obtained from a full optimization of **2** as an unrestricted triplet. The lowest triplet state of $[Ru(bpy)_3]^{2+}$ was also obtained in this way. This particular part of the investigation is presented with the caveat that it assumes that the unrestricted triplet calculations yield reasonable descriptions of the lowest triplet state, although this is not the overall ground state. It can be noted that, although DFT in a strict sense is only a ground-state theory, it has been successfully applied also to studies of the potential energy surfaces of several spin states, for example, of organometallic complexes, where good agreement with experimental findings has been observed. At least from a practical point of view, DFT methods can often be used to explore the energetically lowest lying state of each space or spin irreducible representation of that system.[43]

All considered states of $[Ru(bpy)_3]^{2+}$ and **2** were optimized with and without counter ions in the gas phase. Unless noted otherwise, results presented below for the complexes without explicit counter ions were obtained from gas-phase optimized geometries, while results for systems containing explicit counter ions are for systems in which the counter ions were included in the gas-phase optimizations. Attempts to optimize the complexes with the acetonitrile PCM continuum solvent model were abandoned due to excessive computational times caused in part by erratic convergence of the total energy during the geometry optimizations. For $[Ru(bpy)_3]^{2+}$ and **2**, TD-DFT calculations were performed in the presence of the counter ions and/or with a PCM description of acetonitrile (CH_3CN, $\epsilon = 36.64$) solvent. The solvent calculations for **2** were also extended to benzene (C_6H_6, $\epsilon = 2.247$) and ethanol (CH_3CH_2OH, $\epsilon = 24.55$) to span a wider range of environments, for example, in terms of different dielectric constants.

Finally, some TD-DFT calculations in the gas phase and acetonitrile solvent using different combinations of DFT functionals (B3LYP,[39] BLYP,[44] HCTH,[45] PBE1PBE[46]) and ECP/basis set combinations (LANL2DZ,[40] CEP-31,[47] CEP-121,[47] and SDD[48]) were performed on the B3LYP/LANL2DZ gas-phase optimized geometry of **2** to test the robustness of the calculated electronic properties.

Results

(a) Influence of Rod Length and Conjugation on Optical Ground-State Absorption. Ground-state absorption spectra of complexes with electronically inert substituents are expected to resemble the spectrum of the parent complex closely. Experimentally it has, however, been observed that functionalization of $[Ru(bpy)_3]^{2+}$ with different OPE rigid rods influences the experimental absorption spectra significantly in the visible region.[49,22] Here, we present TD-DFT calculated absorption spectra to provide detailed theoretical information concerning the nature of the different excitations. TD-DFT spectra of $[Ru(bpy)_3]^{2+}$ and **1**−**3** in acetonitrile are presented in Figure 3a, and experimental absorption spectra in acetonitrile are shown in Figure 3b. Characterizations and theoretical assignments of selected important excitations in the absorption spectra of the complexes are summarized in Table 1.

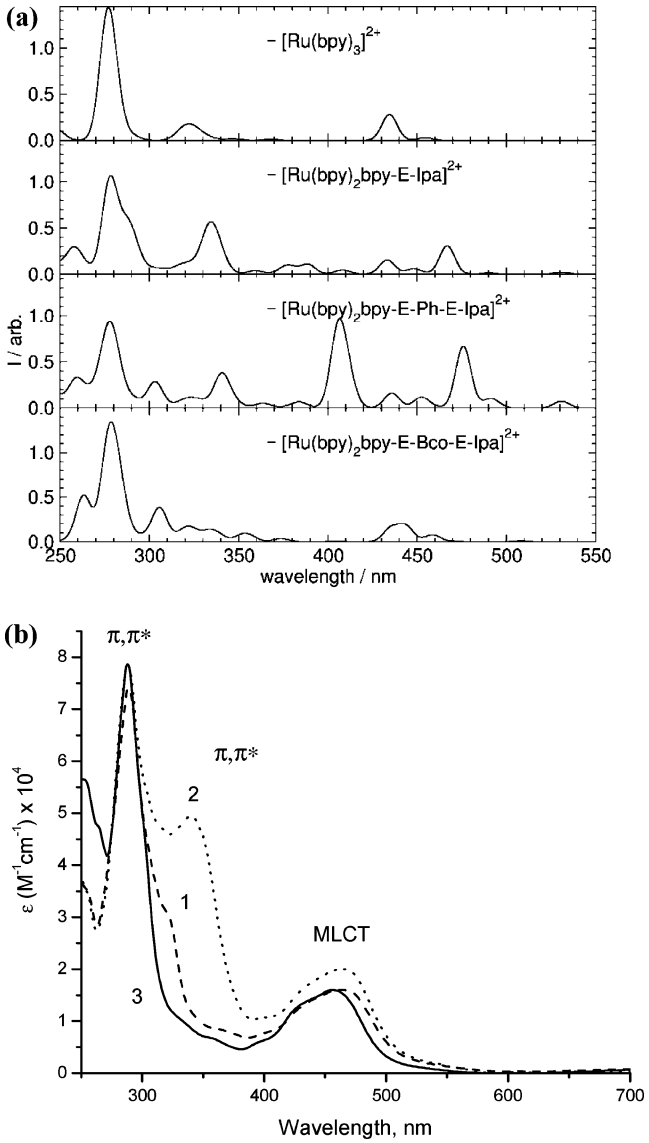

Figure 3. (a) Calculated (TD-DFT) ground-state absorption spectra for $[Ru(bpy)_3]^{2+}$, $[Ru(bpy)_2bpy\text{-}E\text{-}Ipa]^{2+}$ (**1**), $[Ru(bpy)_2bpy\text{-}E\text{-}Ph\text{-}E\text{-}Ipa]^{2+}$ (**2**), and $[Ru(bpy)_2bpy\text{-}E\text{-}Bco\text{-}E\text{-}Ipa]^{2+}$ (**3**) in acetonitrile. (b) Experimental ground-state absorption spectra for complexes **1**−**3** adapted from ref 22.

Particular attention is given to the lowest excited states, for example, by discussing absorption thresholds. The lowest excited states are especially important for the optoelectronic properties of these complexes as these states are frequently reached directly upon photoexcitation or as intermediates following the initial (typically ~100 fs) intermolecular electronic relaxation (via, e.g., internal vibrational relaxation or internal conversion), but prior to subsequent intermolecular or interfacial electron-transfer processes.

The TD-DFT spectral calculations have been performed on the B3LYP/LANL2DZ gas-phase optimized geometries using the PCM description of acetonitrile. The solvent effects were included in the calculations to ensure that the calculations are compatible with the typical experimental conditions under which

TABLE 1: Information Concerning Selected Peaks in the Simulated (TD-DFT) Absorption Spectra of $[Ru(bpy)_3]^{2+}$, 1, 2, and 3 in Acetonitrile[a]

molecule	λ_{exp}[b]/nm	λ_{calc}/nm	f_{calc}	assignment
$[Ru(bpy)_3]^{2+}$		493	0.0003	MLCT threshold
	450	435[c]	0.2772	MLCT maximum
		324[c]	0.0986	MLCT
	~290	276[c]	1.0110	bpy $\pi\rightarrow\pi^*$
$[Ru(bpy)_2bpy\text{-}E\text{-}Ipa]^{2+}$ (**1**)		532	0.0199	MLCT threshold
	462	467[c]	0.3074	MLCT maximum
	325	333[c]	0.3204	$\pi\rightarrow\pi^*$ on rigid rod ligand
	~290	277[c]	0.7881	bpy $\pi\rightarrow\pi^*$
$[Ru(bpy)_2bpy\text{-}E\text{-}Ph\text{-}E\text{-}Ipa]^{2+}$ (**2**)		531	0.0733	MLCT threshold
	465	476[c]	0.6702	MLCT maximum
	~350	406[c]	0.8489	MLCT and $\pi\rightarrow\pi^*$(rod) mix
		341[c]	0.2429	$\pi\rightarrow\pi^*$(rod) and MLCT mix
	~290	279	0.2197	bpy $\pi\rightarrow\pi^*$
$[Ru(bpy)_2bpy\text{-}E\text{-}Bco\text{-}E\text{-}Ipa]^{2+}$ (**3**)		508	0.0085	MLCT threshold
	456	444[c]	0.1733	MLCT maximum
		306[c]	0.3540	bpy $\pi\rightarrow\pi^*$ with some MLCT
	~290	277[c]	0.8872	bpy $\pi\rightarrow\pi^*$

[a] For each peak, the experimental absorption maximum, λ_{exp}, calculated wavelength, λ_{calc}, calculated oscillator strength, f_{calc}, and its calculated assignment are listed. [b] From ref 22. [c] A peak that according to the calculations is composed of two or more essentially isoenergetic excitations with significant oscillator strengths, of which the contribution with the strongest oscillator strength is listed.

the optical and electrochemical properties are measured. The influence of the chemical environment is discussed further below. The number of states included in the TD-DFT calculations has in each case been adjusted to include all excitations with wavelengths down to 250 nm. This typically required approximately 100 states to be included.

$[Ru(bpy)_3]^{2+}$. The absorption spectrum of $[Ru(bpy)_3]^{2+}$ has been studied extensively both experimentally[3] and theoretically.[29−33] As the parent complex of the dyes containing OPE rods, it is included here mainly for comparative purposes. Briefly, it consists of a characteristic broad low-energy metal-to-ligand charge transfer (MLCT) band, involving the excitation of an electron in a Ru 4d t_{2g} orbital to the first unoccupied bpy π^* molecular orbital, in the visible region (400−500 nm), and bpy ligand centered (LC) $\pi\rightarrow\pi^*$ excitations ~290 nm. Our TD-DFT calculation reproduces the MLCT and $\pi\rightarrow\pi^*$ features of the experimental spectrum reasonably well; see Figure 3 and Table 1. In particular, the MLCT maximum is calculated to lie at 435 nm, which can be compared to the experimental value of 450 nm reported by Wang et al.[22] Also, the strong band of LC (bpy) $\pi\rightarrow\pi^*$ excitations experimentally found around 290 nm by Wang et al.[22] is calculated to have its strongest individual contribution at 276 nm. The wavelengths of the two main features are therefore reproduced by the calculations to within 15 nm. The results are also in good agreement with the previous theoretical calculations.[29−33]

$[Ru(bpy)_2bpy\text{-}E\text{-}Ipa]^{2+}$ (1). Complex **1** contains a short, conjugated rigid rod. In the optimized geometry used here, the plane of the Ipa group is planar with the bipyridyl ligand to which the rigid rod is attached. The calculated absorption spectrum of **1**, shown in Figure 3a and with selected excitations listed in Table 1, in many respects resembles that of $[Ru(bpy)_3]^{2+}$ closely, even if the presence of the rigid rod breaks the symmetry of the three bipyridyl ligands present in the parent complex. The absorption threshold for the first singlet−singlet excitation is calculated to lie at 532 nm, which is red-shifted by 39 nm as compared to $[Ru(bpy)_3]^{2+}$. The red-shifted absorption threshold of **1** as compared to $[Ru(bpy)_3]^{2+}$ is according to the calculations due to a delocalization of the lowest unoccupied molecular orbital (LUMO) involved in the low-energy MLCT excitations, as compared to the corresponding LUMO of $[Ru(bpy)_3]^{2+}$. The LUMO is shown in Figure 4a to be strongly delocalized, with significant contributions both on the bpy to which the rigid rod is attached and on the rigid rod. As such, it fits well with a red-shifted MLCT excitation. This delocalization can, furthermore, be expected to promote long-range electron transfer across the bridge, for example, to a TiO_2 substrate, similar to what has been observed in related systems with strong delocalization of the LUMO across the spacer.[23] It can be seen from Figure 3a that the calculated absorption maximum of the MLCT feature is close to the strongest individual MLCT excitation at 467 nm. This is in very good agreement with the experimentally reported value of 462 nm.[22] Both experiments and calculations indicate a red-shift of the MLCT feature as compared to the parent $[Ru(bpy)_3]^{2+}$ complex, although this shift is apparently somewhat exaggerated by the calculations (32 nm according to the calculations as compared to the experimental value of 12 nm[22]). The red-shift is mainly caused by delocalization of the frontier molecular orbitals involved in the excitation. The exaggeration of the red-shift by

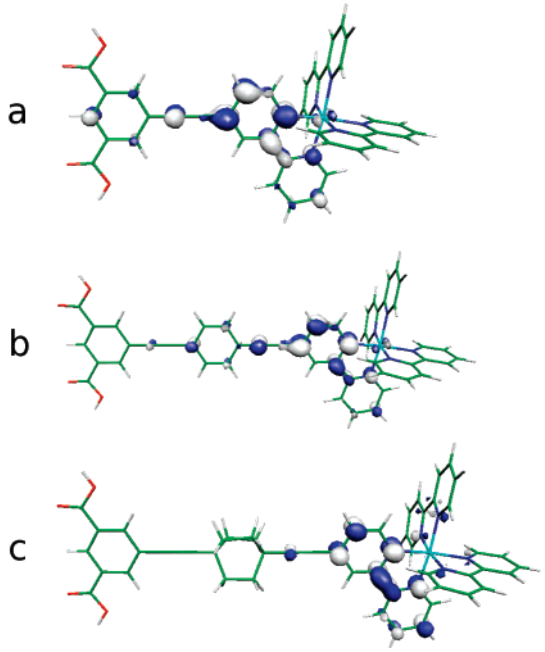

Figure 4. Lowest unoccupied molecular orbital (LUMO) of (a) $[Ru(bpy)_2bpy\text{-}E\text{-}Ipa]^{2+}$ (**1**), (b) $[Ru(bpy)_2bpy\text{-}E\text{-}Ph\text{-}E\text{-}Ipa]^{2+}$ (**2**), and (c) $[Ru(bpy)_2bpy\text{-}E\text{-}Bco\text{-}E\text{-}Ipa]^{2+}$ (**3**) in acetonitrile.

the calculations is probably due, at least to a significant extent, to the fact that the maximally conjugated optimized planar geometry is used, while the rigid rod is likely to have significant rotational freedom under experimental conditions, due to a low torsional barrier for rotation of the phenyl rings of less than 1 kcal/mol.[50,51] The importance of the torsional conformation of electronic delocalization effects through an OPE system has recently been analyzed by Smalley et al.[28] The position of the strong bpy-centered $\pi\rightarrow\pi^*$ excitation at ~290 nm is again well reproduced by the calculations, which predict it to lie at 277 nm. This peak that is assigned to the ancillary bpy ligands is essentially unshifted as compared to the result for $[Ru(bpy)_3]^{2+}$ according to both experiments and calculations. In the calculations, there are several new peaks with moderate intensity in between the MLCT excitations above 400 nm and the bpy $\pi\rightarrow\pi^*$ below 300 nm as compared to the $[Ru(bpy)_3]^{2+}$ spectrum. The strongest peak is calculated to lie at 333 nm. These features can be ascribed mainly to excitations involving delocalized $\pi\rightarrow\pi^*$ bands on the rigid rod functionalized bpy-ligand. This agrees well with the experimental observations of such a band at ~350 nm.[22]

$[Ru(bpy)_2$bpy-E-Ph-E-Ipa$]^{2+}$ (2). A gas-phase optimization of complex **2** resulted in an optimized structure in which the rigid rod extends in a planar fashion from the bipyridyl ligand to which it is attached. As indicated in Table 1, the absorption threshold of **2** is very similar to that of **1**. Figure 4b also shows that, unlike the LUMO of complex **1**, the LUMO of complex **2** does not extend across the complete rigid rod. Apparently, the phenyleneethynylene units are only partly promoting delocalization of the LUMO. The lack of delocalization of the LUMO across the full length of the bridge can be expected to weaken the interfacial electronic coupling with this molecule attached, for example, to a TiO_2 substrate.

The increase of rigid rod length from **1** to **2** does, however, result in a much stronger absorption peak around 350 nm in the experimental spectrum (see Figure 3b). The increased absorption between the MLCT and the ligand $\pi\rightarrow\pi^*$ features of the parent complex can be seen in the calculated spectrum shown in Figure 3a. According to the calculations listed in Table 1, the new strong absorption features in the 300−420 nm range mainly correspond to $\pi\rightarrow\pi^*$ excitations in the rod, which mix with MLCT excitations in the long-wavelength region above ca. 400 nm. In addition, the experimental[22] and calculated spectra again contain a low-energy MLCT band around 450−500 nm and a ligand $\pi\rightarrow\pi^*$ excitation around ~290 nm.

The presence of low-energy excitations on the conjugated rigid rods is a sign that the rod cannot be used as an electronically inert spacer. It can instead be expected to provide electronic levels energetically close to the chromophore frontier orbitals. Although there are a number of new absorption peaks calculated between the MLCT and bpy ligand $\pi\rightarrow\pi^*$ excitation bands, the intensity distribution does not match the new experimental peak appearing at ca. 350 nm closely.[22] As already discussed above for **1**, this can in part depend on the fact that the here optimized planar geometry is distorted by thermal fluctuations under ordinary experimental conditions. As discussed below, the detailed appearance of the absorption spectrum also depends on the modeling of the chemical environment. The electronic structure as well as optical and redox properties of this complex are discussed in greater detail below.

$[Ru(bpy)_2$bpy-E-Bco-E-Ipa$]^{2+}$ (3). Complex **3** was optimized to a geometry in which the Ipa group is oriented in the same plane as the bipyridyl group to which the rigid rod is attached. The E-Bco-E-Ipa spacer, containing one bicyclo[2.2.2]octylene (Bco) unit instead of a phenylene unit, is almost exactly as long as the E-Ph-E-Ipa spacer. As seen in Figure 3, the absorption spectrum of complex **3** appears much more similar to that of $[Ru(bpy)_3]^{2+}$ than does the spectrum of complex **2**. In particular, the MLCT peak is less red-shifted, and the rod-centered peak in the 300−400 nm range is missing. The conjugation of the LUMO level is also seen in Figure 4c to be abruptly broken at the Bco unit. Together, these results show that the saturated Bco unit breaks the π-conjugation more effectively than does the phenylene unit in **2**. Insertion of Bco groups into rigid rods is thus likely to slow down long-range electron-transfer processes across the saturated rigid rods.

TABLE 2: Calculated Absorption Thresholds (nm) in the Gas Phase and in Acetonitrile for the Investigated Complexes

molecule	gas phase	CH_3CN
$[Ru(bpy)_3]^{2+}$	490.03	493.50
$[Ru(bpy)_2$bpy-E-Ipa$]^{2+}$ (**1**)	511.19	530.91
$[Ru(bpy)_2$bpy-E-Ph-E-Ipa$]^{2+}$ (**2**)	811.63	530.85
$[Ru(bpy)_2$bpy-E-Bco-E-Ipa$]^{2+}$ (**3**)	1005.78	508.23

(b) Influence of the Chemical Environment. The main features of the optical absorption spectrum of the extensively studied $[Ru(bpy)_3]^{2+}$ parent complex, the ~290 nm ligand centered $\pi\rightarrow\pi^*$ peak and the ~450 nm MLCT excitation, are generally not strongly affected by the environment. This is illustrated by the similarities in the calculated absorption thresholds in the gas phase (490 nm) and in acetonitrile (493 nm) listed in Table 2. This agrees with published information on this complex.[3] It is therefore tempting to assume that metal complexes derived from this parent complex, such as the here studied complexes carrying rigid rods, would be reasonably accurately characterized computationally without including any treatment of the environment. This would be of significant practical value, as the inclusion of environmental effects in the calculations usually increases the computational cost drastically.

As shown by the absorption thresholds in Table 2, the calculated absorption spectra of **2** and **3** indicate a significant influence by the environment on the optical properties of these two complexes. Notably, the lowest energy excitations for **2** are shifted by inclusion of solvent from 812 to 531 nm, and the corresponding change in **3** is from 1005 to 508 nm. A range of optoelectronic properties of **2**, taken as a model for a complex with a long, conjugated, rigid rod, have therefore been calculated using DFT and TD-DFT calculations in different environments to investigate to what extent the properties of ruthenium polypyridine dyes carrying rigid rods are sensitive to the immediate surroundings, and whether the theoretical modeling is capable of providing a physically realistic description of the complexes with extended conjugation.

(i) Ground-State Electronic Structure. Calculated Mulliken charges of the Ru ion, Q[Ru(II)], in $[Ru(bpy)_3]^{2+}$ and **2** in different chemical environments are compared in Table 3. This shows that Q[Ru(II)] for **2** is almost independent of the environment, with a value of 0.89 both in the gas phase and for all tested solvents. The inclusion of two PF_6^- counter ions only changes the Q[Ru(II)] value slightly to 0.86 in the gas phase and 0.87 in acetonitrile. The Q[Ru(II)] values for $[Ru(bpy)_3]^{2+}$ in four different chemical environments are included for comparison in Table 3, and the result is in both cases identical or highly similar to those of **2**. The interpretation of the Mulliken charges is supported by calculations also of charges from the Natural Population Analysis (NPA) scheme, as listed in Table SI1 in the Supporting Information, although the NPA charges are systematically lower (0.62−0.64) than the Mulliken

TABLE 3: Calculated Mulliken Charges, *Q*, and Spin Densities, SD, for $[Ru(bpy)_3]^{2+}$ and $[Ru(bpy)_2bpy\text{-}E\text{-}Ph\text{-}E\text{-}Ipa]^{2+}$ (2) in the Gas Phase and Selected Chemical Environments

molecule	environment	*Q*[Ru(II)]	*Q*[Ru(III)]	SD[Ru(III)]
$[Ru(bpy)_3]^{2+}$	gas phase	0.89	0.96	0.98
	CH_3CN	0.89	0.98	0.97
	$2PF_6^-$	0.87	0.95	0.97
	$2PF_6^-/CH_3CN$	0.87	0.96	0.98
$[Ru(bpy)_2bpy\text{-}E\text{-}Ph\text{-}E\text{-}Ipa]^{2+}$ (**2**)	gas phase	0.89	0.89	0.05
	C_6H_6	0.89	0.89	0.12
	CH_3CH_2OH	0.89	0.96	0.74
	CH_3CN	0.89	0.97	0.78
	$2PF_6^-$	0.86	0.92	0.93
	$2PF_6^-/CH_3CN$	0.87	0.92	0.96

charges. Together, these findings suggest that the ground-state electronic structure of complex **2** is largely unaffected by the environment. In particular, neither the rigid rod itself, nor the presence of solvents or counter ions changes the Ru ion from the Ru(II) state found in typical Ru polypyridine dyes. It is particularly noteworthy that both the gas phase and the acetonitrile calculations explicitly including two PF_6^- counter ions assign enough negative charge to these counter ions for the calculated Mulliken charge on the Ru(II) ion not to change by more than 0.04 as compared to the corresponding calculations without explicit counter ions.

A visual comparison of the HOMO and the LUMO of **2** in the gas phase and in acetonitrile in Figure 5 does, however, in addition to the obvious shift in absolute energy, reveal a clear difference in the energetic ordering of the frontier orbitals in different environments. Although the Mulliken charge analysis described above suggests that essentially the same orbitals are occupied and unoccupied in the different environments, the internal ordering among the occupied and unoccupied orbitals is seen to change significantly between the gas phase and the acetonitrile cases. In the gas phase, the HOMO is located on the rigid rod and the LUMO is located on the auxiliary bpy ligands. In the presence of acetonitrile, the HOMO is instead located mainly on the Ru(II) ion, and the LUMO is located on the substituted bpy ligand, with parts of the electron distribution stretching out onto the rigid rod. The clear changes in HOMO and LUMO appearances with inclusion of the chemical environment in the calculations are strong indications that the surrounding is capable of influencing the optical and electrochemical properties of the dyes carrying rigid rods, as the HOMO and LUMO levels are usually actively involved in both redox reactions and optical excitations.

The sensitivity of the complexes carrying the OPE rods to the environment arises from π and π^* levels on the rigid rod that form bands with a relatively small energy gap between the occupied and unoccupied levels, so that the frontier orbitals of the rod appear at energies similar to those of the chromophore frontier orbitals. The reason that the relative ordering of the molecular orbitals actually changes is likely to be that the positive charge on the metal ion is preferentially screened when the environment is included. While perhaps somewhat unrealistic under ordinary experimental electrochemical conditions, the charge of a naked Ru(II) ion leads to a drastic stabilization of nearby orbitals. This clearly includes the Ru 4d orbitals, but apparently also the bpy π and π^* levels to a large degree. This explains why the $[Ru(bpy)_3]^{2+}$ complex is not strongly affected by environmental effects: the ordering of the bpy π and π^* levels relative to the Ru 4d t_{2g} and e_g orbitals is largely unaffected by the solvent, although all molecular orbitals are strongly stabilized energetically when the Ru(II) is unscreened. However, the frontier orbitals of the rigid rods are less affected by the screening of the Ru(II) ion. This leads to a rearrangement of the molecular orbitals when the environment is taken into account. For example, Figure 5 shows that both the HOMO and the LUMO of **2** are changed drastically between the gas phase and the acetonitrile calculations. In the gas phase, the Ru t_{2g} levels have been pulled down in energy sufficiently to allow several occupied molecular orbitals on the rod to appear higher in energy. In fact, the highest MO with significant Ru contributions is HOMO−4. In acetonitrile, this order is reversed, so that the Ru t_{2g} levels are again found as the highest occupied MOs. Although less pronounced, the ordering of the first unoccupied MOs is also changed when going from the gas phase to acetonitrile. It is clear that the environment must be included in the calculations to obtain realistic electronic structures of the complexes containing rigid rods. Also, these results suggest that optoelectronic properties of these complexes, such as the efficiency of photoinduced electron injection to a substrate, for example, TiO_2, can be tuned by changing the chemical environment.

(ii) Optical Absorption. The influence of the environment on TD-DFT calculated absorption spectra has also been investigated, and calculated TD-DFT spectra for different environments are displayed for $[Ru(bpy)_3]^{2+}$ and **2** in Figure 6a and b, respectively. The corresponding absorption thresholds for **2** are listed in Table 4.

As expected from the results discussed above, the calculated absorption spectrum of $[Ru(bpy)_3]^{2+}$ is hardly affected by the environment, as shown in Figure 6a. In contrast, the gas-phase spectrum of **2** contains spurious low-energy excitations, with a threshold at 812 nm. The low-energy excitations correspond to charge-transfer excitations of, for example, HOMO→LUMO character that take an electron from the rod and populate an orbital localized on the $Ru(bpy)_3$ chromophore. Although clearly not compatible with experimental results measured in solution, the charge-transfer excitations found here are not necessarily unphysical in the gas phase with the unscreened Ru(II). As shown in Figure 6b, inclusion of solvents with a wide range of dielectric constants alters the calculated absorption spectrum significantly. In particular, the peaks with long wavelengths in the gas-phase spectrum disappear. Instead, the spectrum looks much more similar to the parent $[Ru(bpy)_3]^{2+}$ chromophore spectrum, which starts with MLCT excitations on the chromophore around 500 nm. This shows that the screening by the solvent removes the spurious low-energy charge-transfer excitations that reduce the chromophore, rather than oxidize it as is the usual photoinduced redox mechanism in this kind of complex.

TD-DFT spectra were also calculated on the combined system comprising complex **2** together with two PF_6^- counter ions explicitly included in the calculation. TD-DFT absorption spectra were calculated both in the gas phase and in acetonitrile using the geometry from a gas-phase optimization of the system containing both the complex and the two counter ions. The $\mathbf{2}(PF_6^-)_2$ system has a calculated excitation threshold at 614 nm in the gas phase, which is significantly shorter than for the corresponding threshold of the complex without counter ions. In contrast, the threshold with counter ions in acetonitrile is calculated at 563 nm, which is longer than the 531 nm value for the chromophore in acetonitrile but without the counter ions. Thus, inclusion of both solvents and counter ions influences the TD-DFT spectrum significantly for this complex, and the spectrum including both counter ions and acetonitrile solvent has an intermediate threshold as compared to including either

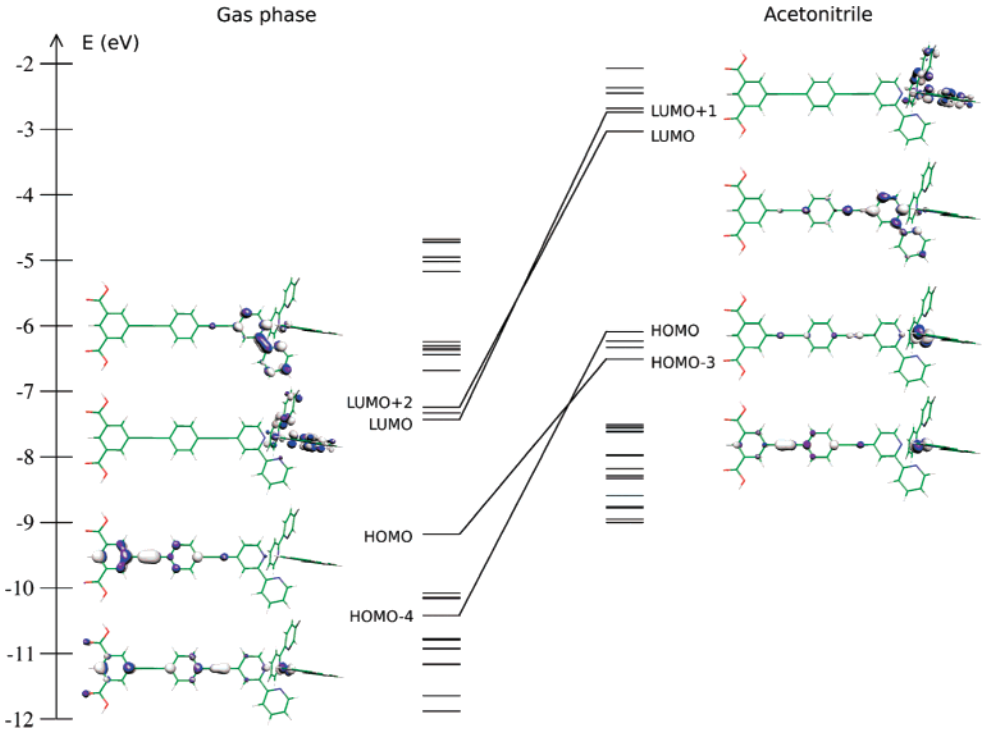

Figure 5. Molecular orbital (MO) diagram of $[Ru(bpy)_2bpy\text{-}E\text{-}Ph\text{-}E\text{-}Ipa]^{2+}$ (**2**) in the gas phase (left) and in acetonitrile (right).

one or the other. To some extent, both solvent and counter ions screen the positive Ru(II) ion in such a way as to remove the spurious long wavelength excitations seen for the bare chromophore.

The method sensitivity of the electronic properties, and in particular the low-energy excitations, was tested further by comparing the calculated absorption thresholds of complex **2** for several different functionals (B3LYP, BLYP, HCTH, PBE1PBE) together with the LANL2DZ ECP and accompanying basis set, and for the B3LYP functional together with several different ECP/basis sets (LANL2DZ, CEP-31, CEP-121, and SDD) both in the gas phase and in acetonitrile. These calculations were all performed on the B3LYP/LANL2DZ gas-phase optimized geometry. It is shown in Table 5 that, while the exact thresholds vary considerably for the different method combinations, they all give a substantially more realistic absorption threshold in the presence of the solvent. Thus, the removal of low-energy charge-transfer excitations is seen to be a rather general effect of the inclusion of the environment, and not a random success of the B3LYP/LANL2DZ method. This supports the conclusion that the removal of low-energy charge-transfer excitations could generally be attributed to a similar correction of the frontier molecular orbital alignment as described for the B3LYP/LANL2DZ method combination presented above.

Arguably, it is highly unlikely to find an isolated and doubly charged complex in any ordinary chemical environment. The reason that TD-DFT calculations of charged metal complexes such as for $[Ru(bpy)_3]^{2+}$ often yield reasonably good calculated spectra is then a largely fortuitous lack of low-energy charge-transfer excitations because of the limited system size. Despite the significant additional computational cost, it becomes imperative to include the environment in a realistic way when the systems become more extended, such as in the here investigated complexes carrying rigid rods.

Spurious low-energy excitations in TD-DFT spectra are often considered a hallmark of unphysical charge-transfer excitations in extended systems.[52−62] It would therefore be tempting to discard the low-energy charge-transfer excitations seen in these simulated gas-phase spectra of **2** and **3** as artifact caused by the TD-DFT methodology itself. The fact that these charge-transfer excitations are removed in the more realistic calculations including the environment instead suggests that it may instead sometimes be the physical modeling of the system, rather than the TD-DFT methodology, that is the most important reason for the appearance of spurious low-energy charge-transfer excitations in TD-DFT simulated absorption spectra. It will therefore be interesting to examine other extended systems to see to what extent a better description of the chemical environment can improve TD-DFT simulated absorption spectra for a broader range of extended systems.

The sensitivity of the calculated absorption spectra to the chemical environment finally corroborates the possibilities to utilize changes in the chemical environment, mentioned for the ground-state properties above, to tune the optoelectronic properties of these molecules.

(iii) Triplet State. We have also investigated the triplet state of **2**, as a potentially important intermediate in the photoexcited complex. This state would be reached after internal vibrational relaxation and intersystem crossing of the initially excited state produced by the absorption process, but prior to one-electron oxidation of the complex.

First, the triplet state of **2** was considered in the gas phase, and its calculated spin density is shown in Figure 7. The Mulliken charge and spin density on the Ru ion are listed in Table 6. The resulting spin density of 0.10 on the Ru ion is very different from that expected in an ordinary triplet metal-to-ligand charge transfer (^{3}MLCT) state, as shown by the comparison with the corresponding value of 0.97 for $^3[Ru(bpy)_3]^{2+}$, which is also listed in Table 6. Including solvent effects through a calculation with a PCM description of acetonitrile on the gas-phase optimized triplet state geometry results in a significant change of the Ru spin density to 0.36. This value is significantly closer to that of a typical ^{3}MLCT state, even if it is still far from the values of nearly one obtained for the comparatively pure $^3[Ru(bpy)_3]^{2+}$ MLCT state.

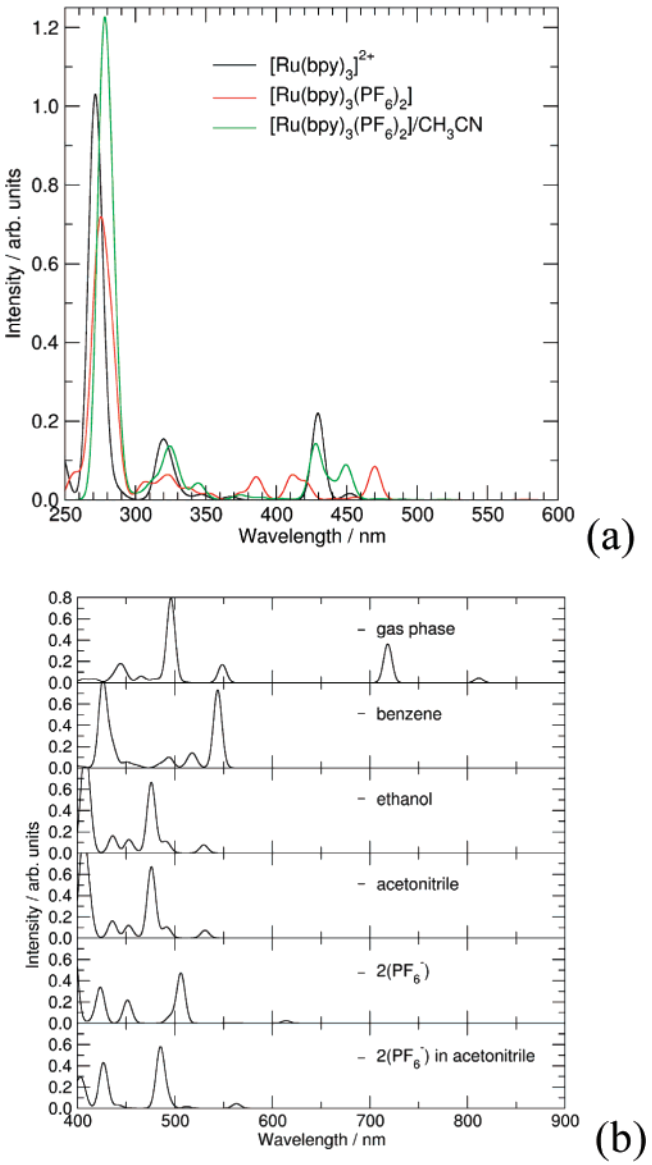

Figure 6. Calculated (TD-DFT) absorption spectra of (a) $[Ru(bpy)_3]^{2+}$ and (b) $[Ru(bpy)_2bpy\text{-}E\text{-}Ph\text{-}E\text{-}Ipa]^{2+}$ (**2**) in different environments.

TABLE 4: Calculated Absorption Thresholds, λ_{calc} (nm), and Corresponding Oscillator Strengths, f_{calc}, for $[Ru(bpy)_2bpy\text{-}E\text{-}Ph\text{-}E\text{-}Ipa]^{2+}$ (2) in Different Environments

environment	λ_{calc}	f_{calc}
gas phase	811.64	0.0431
C_6H_6	543.82	0.7341
CH_3CH_2OH	529.59	0.0775
CH_3CN	530.85	0.0733
$2PF_6^-$	614.15	0.0243
$2PF_6^-/CH_3CN$	563.02	0.0439

As the electronic state is seen to change significantly by the environment in these particular complexes, it is questionable if the gas-phase optimized geometry is a good representation of the triplet state geometry. The popular approach to include, for example, solvent effects in single point calculations on gas-phase optimized geometries is therefore unlikely to yield an accurate description of the geometry, and it is difficult to assess to what extent the calculated electronic properties are affected. Therefore, a triplet state geometry of the complex was obtained from a vacuum calculation explicitly including two PF_6^- counter ions in the optimization. This results in optimized ^{3}MLCT states with Mulliken spin densities reported in Table 6 as 0.84 and 0.90 in the gas phase and acetonitrile, respectively. The resulting spin density with counter ions in acetonitrile is also shown in Figure 7, where it can be clearly seen that this represents a very different electronic state as compared to the gas-phase triplet.

TABLE 5: Calculated Absorption Thresholds (nm) for $[Ru(bpy)_2bpy\text{-}E\text{-}Ph\text{-}E\text{-}Ipa]^{2+}$ (2) in the Gas Phase and Acetonitrile with Different DFT Functionals and ECP/Basis Sets

method	gas phase	CH_3CN
B3LYP/LANL2DZ	811.64	530.85
B3LYP/CEP-31	792.03	526.82
B3LYP/CEP-121	782.61	527.45
B3LYP/SDD	816.33	553.88
BLYP/LANL2DZ	1804.13	723.98
HCTH/LANL2DZ	1722.15	738.28
PBE1PBE/LANL2DZ	697.29	500.45

The amount of spin density on the ruthenium ion given in Table 6 for various environments can apparently be successfully correlated to the degree to which an electron is removed from one of the Ru 4d t_{2g} orbitals in the triplet state and is as such an important indicator of the nature of the triplet state. The results based on Mulliken charges and spin densities are corroborated by highly similar results obtained from NPA calculations, as listed in Table SI2 of the Supporting Information.

(iv) Oxidation. Finally, the redox reaction that is most relevant to the use of these dyes is the photooxidation that formally leads to a Ru(III) state. To study this, the geometry of the oxidized (net charge +3) form of complex **2** was initially optimized in the gas phase. The Mulliken charge of the Ru(III) ion, *Q*[Ru(III)], and the corresponding Mulliken spin density SD[Ru(III)] were calculated in different environments and listed in Table 3. Here, the Mulliken population analysis reveals larger differences depending on the environment as compared to the normal Ru(II) oxidation state of the complex. The *Q*[Ru(III)] charge increases from 0.89 to 0.97 from the gas phase to the acetonitrile case, and with benzene and ethanol giving intermediate values. For $[Ru(bpy)_3]^{3+}$, the corresponding values are 0.96 and 0.98, respectively, which is a somewhat smaller difference. A still more pronounced effect is seen in the spin density analysis, where the SD[Ru(III)] goes from 0.05 to 0.96 for the oxidized complex **2** in the gas phase and in acetonitrile with two PF_6^- counter ions, respectively. The gas-phase value of 0.05 indicates that the unpaired spin does not reside on the Ru ion, whereas the value of 0.96 suggests that it does. Figure 5 shows that, in the gas phase, the electron is largely removed from the rod frontier orbital, whereas in the presence of the solvents with high dielectric constants and/or counter ions it is largely removed from the Ru ion. This is corroborated by the spin density plots for the oxidized state in two different environments shown in Figure 7. The SD[Ru(III)] values for $[Ru(bpy)_3]^{3+}$ are 0.98 and 0.98 in the gas phase and in acetonitrile with counter ions, respectively. Thus, in the $[Ru(bpy)_3]^{3+}$ case there is no corresponding ambiguity as the electron is always taken from the Ru ion. The Mulliken charge and spin density analysis are supported from NPA results listed in Table SI1 in the Supporting Information.

As for the triplet case, the fact that the environment is so critical to obtain a realistic description of the electronic state of the oxidized complex makes the optimizations that do not include any environmental effects questionable. In this case, the geometry of the oxidized complex is optimized in the gas phase to a state with an electron hole on the rigid rod, whereas the solvents partly stabilize the hole on the ruthenium ion even at this geometry that should be particularly favorable for the state to which it was optimized. Judging from the calculated

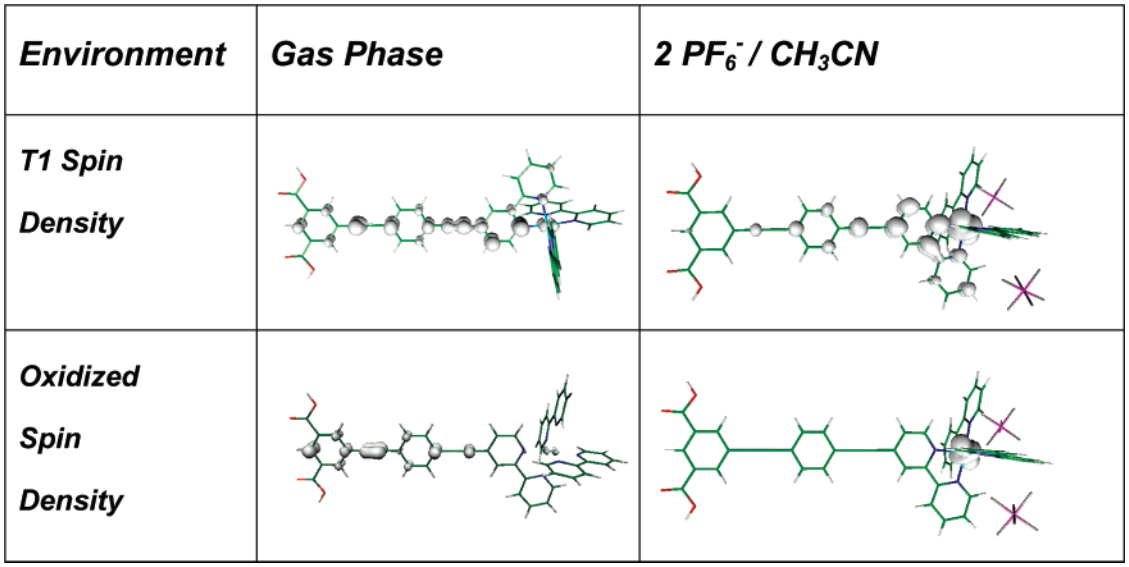

Figure 7. Calculated spin densities of the triplet (T1) state and the oxidized state of $[Ru(bpy)_2bpy\text{-}E\text{-}Ph\text{-}E\text{-}Ipa]^{2+}$ (**2**) in the gas phase and with two PF_6^- counter ions in acetonitrile.

TABLE 6: Calculated Mulliken Charges, *Q*, and Spin Densities, SD, at the Ru Center of $^3[Ru(bpy)_3]^{2+}$ and $^3[Ru(bpy)_2bpy\text{-}E\text{-}Ph\text{-}E\text{-}Ipa]^{2+}$ (2) for the Lowest Triplet States in Different Environments

molecule	environment	*Q*(Ru)	SD(Ru)
$^3[Ru(bpy)_3]^{2+}$	gas phase	0.98	0.97
$^3[Ru(bpy)_2bpy\text{-}E\text{-}Ph\text{-}E\text{-}Ipa]^{2+}$(**2**)	gas phase	0.90	0.10
	CH_3CN	0.95	0.36
	$2PF_6^-$	0.93	0.84
	$2PF_6^-/CH_3CN$	0.94	0.90

TABLE 7: Calculated Oxidation Energies (eV) for $[Ru(bpy)_3]^{2+}$ and $[Ru(bpy)_2bpy\text{-}E\text{-}Ph\text{-}E\text{-}Ipa]^{2+}$ (2) in Different Environments

environment	$[Ru(bpy)_3]^{2+}$	$[Ru(bpy)_2bpy\text{-}E\text{-}Ph\text{-}E\text{-}Ipa]^{2+}$
gas phase	12.04	10.25
CH_3CN	5.84	5.92
$2PF_6^-$	7.09	7.02
$2PF_6^-/CH_3CN$	5.62	5.64

Ru Mulliken spin density, the optimization in the presence of counter ions results in a geometry which together with the stabilizing effects of counter ions and solvents localize the electron hole on the ruthenium ion. In other words, a formally oxidized Ru(III) ion center is created.

Adiabatic oxidation energies of $[Ru(bpy)_3]^{2+}$ and **2**, obtained as the differences in total energies between the oxidized (III) and reduced (II) states of the relevant systems, were also calculated in different environments, and the results are listed in Table 7. The listed values are adiabatic energies from the optimizations in the gas phase with or without counter ions, as appropriate. The oxidation energy for $[Ru(bpy)_3]^{2+}$ and **2** differ by about 2 eV according to the gas-phase calculations. In the presence of acetonitrile, the oxidation energies are in both cases reduced to ca. 5.9 eV, which in both cases represents a significant reduction of the oxidation energy as compared to the gas-phase result. The reductions of the oxidation energies arise from the additional stabilization of the positive charge of the complex, the effect of which is largest for the more highly charged oxidized state. The inclusion of counter ions in the calculations with and without solvents also leads to oxidation energies, which are very similar for the two complexes. Experimentally, the oxidation potentials of the two dyes are similar, which supports the correctness of the calculations that include environmental effects. Conversely, the gas-phase calculations again appear to give an incorrect description of the physically observable quantities involved.

The large differences in the calculated electronic state for the oxidized molecules in different chemical environments, for example, with and without counter ions, also have more practical implications in terms of the electrochemical properties. The calculations suggest that the oxidation properties of these dye molecules can be substantially different in different chemical environments.

Conclusions

The modification of ruthenium tris-bipyridine dyes by OPE rigid rods is seen to have significant effects on the calculated electronic structure of the investigated ruthenium dyes. Spectral and electrochemical properties are, in particular, influenced by the delocalization of molecular orbitals on the functionalized bpy ligand onto the rigid rod. This gives rise to significant changes in the absorption spectra of these complexes as compared to the absorption spectrum of the Ru tris-bipyridine dye by itself.

Furthermore, the calculated electronic properties are found to be much more sensitive to the surrounding for the complexes carrying rigid rods as compared to the situation for the parent complex. The quantum chemical description of the excitation properties of complex **2** is in good agreement with the published experimental information for this complex, with a realistic description of both the optical absorption spectrum and the oxidation, when the chemical environment is included in the calculation. In contrast, the gas-phase calculations result in unphysical low-energy excitations and an oxidation energy that, in contrast to the experiments, is very different from that of $[Ru(bpy)_3]^{2+}$.

To some extent, the modeling of environmental effects can be regarded as a computational problem. In particular, the lack of screening of ionic charges in gas-phase calculations is unrealistic as compared to experimental conditions and causes incorrect descriptions of the electronic states and excitations, including spurious low-energy charge-transfer excitations in TD-DFT calculations. In this respect, it is interesting to note that the spurious low-energy excitations present in the gas-phase calculations disappear with a more realistic treatment of the

chemical environment and are not due to the, often invoked, intrinsic shortcomings of TD-DFT to describe charge-transfer excitations.

The calculated sensitivity of the electronic properties on the environment may also be of interest as a viable route to tune the optoelectronic properties of these systems. For example, when these molecules are attached to a semiconductor such as TiO_2 via the carboxylic acid anchor groups, they can be used to achieve ultrafast photoinduced charge-separation from the chromophore to the semiconductor, involving electron transfer across the rigid rod. By changing the environment, either with different counter ions or solvents with different dielectric constants, it appears to be possible to tune the electronic level alignment between the chromophore and the rigid rod units. This should have a direct influence on the ability of the rigid rods to act as mediators of heterogeneous or supramolecular photoinduced electron-transfer processes.

Acknowledgment. The Göran Gustafsson Foundation and the Swedish Research Council (Vetenskapsrådet) are gratefully acknowledged for financial support. The Swedish National Supercomputer Centre (NSC) is acknowledged for generous grants of computing resources. The Division of Chemical Sciences, Office of Basic Energy Sciences, U.S. Department of Energy, DE-FG02-96ER14662 (G.J.M.) and DE-FG02-01ER15256 (E.G.), is gratefully acknowledged for research support.

Supporting Information Available: Calculated charges and spin densities from Natural Population Analysis (NPA) for selected states of selected complexes. This material is available free of charge via the Internet at http://pubs.acs.org.

References and Notes

(1) Kavarnos, G. J. *Fundamentals of Photoinduced Electron Transfer*; VCH Publishers: New York, 1993.
(2) Meyer, T. J. *Acc. Chem. Res.* **1989**, *22*, 163.
(3) Juris, A.; Balzani, V.; Barigelletti, F.; Campagna, S.; Belser, P.; Vonzelewsky, A. *Coord. Chem. Rev.* **1988**, *84*, 85.
(4) O'Regan, B.; Grätzel, M. *Nature* **1991**, *353*, 737.
(5) (a) Hagfeldt, A.; Grätzel, M. *Chem. Rev.* **1995**, *95*, 49. (b) Kalyanasundaram, K.; Grätzel, M. *Coord. Chem. Rev.* **1998**, *77*, 347.
(6) Hagfeldt, A.; Grätzel, M. *Acc. Chem. Res.* **2000**, *33*, 269.
(7) Miller, R. J. D.; McLendon, G. L.; Nozik, A. J.; Schmickler, W.; Willig, F. *Surface Electron Transfer Processes*; VCH Publishers: New York, 1995.
(8) Tachibana, Y.; Moser, J. E.; Grätzel, M.; Klug, D. R.; Durrant, J. R. *J. Phys. Chem.* **1996**, *100*, 20056.
(9) Hannappel, T.; Burfeindt, B.; Storck, W.; Willig, F. *J. Phys. Chem. B* **1997**, *101*, 6799.
(10) Heimer, T. A.; Heilweil, E. J.; Bignozzi, C. A.; Meyer, G. J. *J. Phys. Chem. A* **2000**, *104*, 4256.
(11) Willig, F.; Zimmermann, C.; Ramakrishna, S.; Storck, W. *Electrochim. Acta* **2000**, *45*, 4565.
(12) Zimmermann, C.; Willig, F.; Ramakrishna, S.; Burfeindt, B.; Pettinger, B.; Eichberger, R.; Storck, W. *J. Phys. Chem. B* **2001**, *105*, 9245.
(13) Schnadt, J.; Bruhwiler, P. A.; Patthey, L.; O'Shea, J. N.; Södergren, S.; Odelius, M.; Ahuja, R.; Karis, O.; Bassler, M.; Persson, P.; Siegbahn, H.; Lunell, S.; Mårtensson, N. *Nature* **2002**, *418*, 620.
(14) Benkö, G.; Kallioinen, J.; Korppi-Tommola, J. E. I.; Yartsev, A. *J. Am. Chem. Soc.* **2002**, *124*, 489.
(15) Huber, R.; Moser, J. E.; Grätzel, M.; Wachtveitl, J. *J. Phys. Chem. B* **2002**, *105*, 9245.
(16) Asbury, J. B.; Hao, E.; Wang, Y.; Lian, T. *J. Phys. Chem. B* **2001**, *105*, 4545.
(17) Persson, P.; Bergström, R.; Ojamäe, L.; Lunell, S. *Adv. Quantum Chem.* **2002**, *41*, 203.
(18) Persson, P.; Lunell, S.; Bruhwiler, P. A.; Schnadt, J.; Södergren, S.; O'Shea, J. N.; Karis, O.; Siegbahn, H.; Mårtensson, N.; Bassler, M.; Patthey, L. *J. Chem. Phys.* **2000**, *112*, 3945.
(19) Galoppini, E. *Coord. Chem. Rev.* **2004**, *248*, 1283.
(20) Asbury, J. B.; Hao, E.; Wang, Y.; Lian, T. *J. Phys. Chem. B* **2000**, *104*, 11957.
(21) Kilså, K.; Mayo, E. I.; Kuciauskas, D.; Villahermosa, R.; Lewis, N. S.; Winkler, J. R.; Gray, H. B. *J. Phys. Chem. A* **2003**, *107*, 3379.
(22) Wang, D.; Mendelsohn, R.; Galoppini, E.; Hoertz, P. G.; Carlisle, R. A.; Meyer, G. J. *J. Phys. Chem. B* **2004**, *108*, 16642.
(23) Persson, P.; Lundqvist, M. J.; Ernstorfer, R.; Goddard, W. A., III; Willig, F. *J. Chem. Theory Comput.* **2006**, *2*, 441.
(24) (a) Lamberto, M.; Pagba, C.; Piotrowiak, P.; Galoppini, E. *Tetrahedron Lett.* **2005**, *46*, 4895. (b) Pietrowiak, P.; Galoppini, E.; Wei, Q.; Meyer, G. J.; Wiewior, P. *J. Am. Chem. Soc.* **2003**, *125*, 5278.
(25) Hoertz, P. G.; Carlisle, R.; Meyer, G. J.; Wang, D.; Piotrowiak, P. Galoppini, E. *Nano Lett.* **2003**, *3*, 325.
(26) Adams, M. D.; Brus, L.; Chidsey, C. E. D.; Creager, S.; Creutz, C.; Kagan, C. R.; Kamat, P. V.; Lieberman, M.; Lindsay, S.; Marcus, R. A.; Metzger, R. M.; Michel-Beyerle, M. E.; Miller, J. R.; Newton, M. D.; Rolison, D. R.; Sankey, O.; Schanze, K. S.; Yardley, J.; Zhu, X. Y. *J. Phys. Chem. B* **2003**, *107*, 6668.
(27) (a) Leroy-Lhez, S.; Parker, A.; Lapouyade, P.; Belin, C.; Ducasse, L.; Oberle, J.; Fages, F. *Photochem. Photobiol. Sci.* **2004**, *3*, 949. (b) Chaignon, F.; Torroba, J.; Blart, E.; Borgström, M.; Hammarström, L.; Odobel, F. *New J. Chem.* **2005**, *29*, 1272. (c) Sudeep, P. K.; James, P. V.; Thomas, K. G.; Kamat, P. V. *J. Phys. Chem. A* **2006**, *110*, 5649.
(28) Smalley, J. F.; Sachs, S. B.; Chidsey, C. E. D.; Dudek, S. P.; Sikes, H. D.; Creager, S. E.; Yu, C. J.; Feldberg, S. W.; Newton, M. D. *J. Am. Chem. Soc.* **2004**, *126*, 14620.
(29) Broo, A.; Lincoln, P. *Inorg. Chem.* **1997**, *36*, 2544.
(30) Buchs, M.; Daul, C. *Chimia* **1998**, *52*, 163.
(31) Gorelsky, S. I.; Lever, A. B. P. *J. Organomet. Chem.* **2001**, *635*, 187.
(32) Zheng, K. C.; Wang, J. P.; Peng, W. L.; Liu, X. W.; Yun, F. C. *J. Mol. Struct. (THEOCHEM)* **2002**, *582*, 1.
(33) Xie, Z. Z.; Fang, W. H. *J. Mol. Struct. (THEOCHEM)* **2005**, *717*, 179.
(34) Fantacci, S.; De Angelis, F.; Selloni, A. *J. Am. Chem. Soc.* **2003**, *125*, 4381.
(35) Guillemoles, J.-F.; Barone, V.; Joubert, L.; Adamo, C. *J. Phys. Chem. A* **2002**, *106*, 11354.
(36) Persson, P.; Lundqvist, M. J. *J. Phys. Chem. B* **2005**, *109*, 11918.
(37) Persson, P.; Bergström, R.; Lunell, S. *J. Phys. Chem. B* **2000**, *104*, 10348.
(38) Brunschwig, B. S.; Ehrenson, S.; Sutin, N. *J. Am. Chem. Soc.* **1987**, *91*, 4714.
(39) Becke, A. D. *J. Chem. Phys.* **1993**, *98*, 5648.
(40) (a) Dunning, T. H., Jr.; Hay, P. J. In *Modern Theoretical Chemistry*; Schaefer, H. F., III, Ed.; Plenum: New York, 1976; Vol. 3. (b) Hay, P. J.; Wadt, W. R. *J. Chem. Phys.* **1985**, *82*, 270. (c) Wadt, W. R.; Hay, P. J. *J. Chem. Phys.* **1985**, *82*, 284. (d) Hay, P. J.; Wadt, W. R. *J. Chem. Phys.* **1985**, *82*, 299.
(41) Frisch, M. J.; Trucks, G. W.; Schlegel, H. B.; Scuseria, G. E.; Robb, M. A.; Cheeseman, J. R.; Montgomery, J. A., Jr.; Vreven, T.; Kudin, K. N.; Burant, J. C.; Millam, J. M.; Iyengar, S. S.; Tomasi, J.; Barone, V.; Mennucci, B.; Cossi, M.; Scalmani, G.; Rega, N.; Petersson, G. A.; Nakatsuji, H.; Hada, M.; Ehara, M.; Toyota, K.; Fukuda, R.; Hasegawa, J.; Ishida, M.; Nakajima, T.; Honda, Y.; Kitao, O.; Nakai, H.; Klene, M.; Li, X.; Knox, J. E.; Hratchian, H. P.; Cross, J. B.; Bakken, V.; Adamo, C.; Jaramillo, J.; Gomperts, R.; Stratmann, R. E.; Yazyev, O.; Austin, A. J.; Cammi, R.; Pomelli, C.; Ochterski, J. W.; Ayala, P. Y.; Morokuma, K.; Voth, G. A.; Salvador, P.; Dannenberg, J. J.; Zakrzewski, V. G.; Dapprich, S.; Daniels, A. D.; Strain, M. C.; Farkas, O.; Malick, D. K.; Rabuck, A. D.; Raghavachari, K.; Foresman, J. B.; Ortiz, J. V.; Cui, Q.; Baboul, A. G.; Clifford, S.; Cioslowski, J.; Stefanov, B. B.; Liu, G.; Liashenko, A.; Piskorz, P.; Komaromi, I.; Martin, R. L.; Fox, D. J.; Keith, T.; Al-Laham, M. A.; Peng, C. Y.; Nanayakkara, A.; Challacombe, M.; Gill, P. M. W.; Johnson, B.; Chen, W.; Wong, M. W.; Gonzalez, C.; Pople, J. A. *Gaussian 03*, revision C.02; Gaussian, Inc.: Wallingford, CT, 2004.
(42) Cossi, M.; Scalmani, G.; Rega, N.; Barone, V. *J. Chem. Phys.* **2002**, *117*, 43.
(43) (a) Koch, W; Holthausen, M. C. *A Chemist's Guide to Density Functional Theory*, 2nd ed.; Wiley-VCH: Weinheim, 2000; p 59. (b) Carreòn-Macedo, J.-L.; Harvey, J. N. *J. Am. Chem. Soc.* **2004**, *126*, 5789.
(44) (a) Becke, A. D. *Phys. Rev. A* **1988**, *38*, 3098. (b) Lee, C.; Yang, W. Parr, R. G. *Phys. Rev. B* **1988**, *37*, 785.
(45) Boese, A. D.; Handy, N. C. *J. Chem. Phys.* **2001**, *114*, 5497.
(46) Adamo, C.; Barone, V. *J. Chem. Phys.* **1999**, *110*, 6158.
(47) (a) Stevens, W.; Basch, H.; Krauss, M. *J. Chem. Phys.* **1984**, *81*, 6026. (b) Stevens, W.; Krauss, M.; Basch, H. *Can. J. Chem.* **1992**, *70*, 612. (c) Cundari, T. R.; Stevens, W. J. *J. Chem. Phys.* **1993**, *98*, 5555.
(48) Dolg, M.; Stoll, H.; Preuss, H.; Pitzer, R. M. *J. Phys. Chem.* **1993**, *97*, 5852.
(49) Wang, Y.; Liu, S.; Pinto, M. R.; Dattelbaum, D. M.; Schoonover, J. R.; Schanze, K. S. *J. Phys. Chem. A* **2001**, *105*, 11118.
(50) Okuyama, K.; Hasegawa, T.; Ito, M.; Mikami, N. *J. Phys. Chem.* **1984**, *88*, 1711.

(51) Seminario, J. M.; Zacarias, A. G.; Tour, J. M. *J. Am. Chem. Soc.* **1998**, *120*, 3970.
(52) Tozer, D. J.; Amos, R. D.; Handy, N. C.; Roos, B. O.; Serrano-Andres, L. *Mol. Phys.* **1999**, *97*, 859.
(53) Fabien, J. *Theor. Chem. Acc.* **2001**, *106*, 199.
(54) Cai, Z.-L.; Sendt, K.; Reimers, J. F. *J. Chem. Phys.* **2002**, *117*, 5543.
(55) Dreuw, A.; Weisman, J.; Head-Gordon, M. *J. Chem. Phys.* **2003**, *119*, 2943.
(56) Tozer, D. *J. Chem. Phys.* **2003**, *19*, 12697.
(57) Liao, M.-S.; Lu, Y.; Scheiner, S. *J. Comput. Chem.* **2003**, *24*, 623.
(58) Dreuw, A.; Head-Gordon, M. *J. Am. Chem. Soc.* **2004**, *126*, 4007.
(59) Gritsenko, O.; Baerends, E. J. *J. Chem. Phys.* **2004**, *121*, 655.
(60) Casida, M. E.; Gutierrez, F.; Guan, J. G.; Gadea, F. X.; Salahub, D.; Daudey, J. P. *J. Chem. Phys.* **2004**, *120*, 8425.
(61) Tawada, Y.; Tsuneda, T.; Yanagisawa, S.; Yanai, T.; Hirao, K. *J. Chem. Phys.* **2004**, *120*, 8425.
(62) Maitra, N. T. *J. Chem. Phys.* **2005**, *122*, 234104.